



OPEN

# Evolution law of surrounding rock stress field for ultra-deep shaft development blasting

Bo Sun<sup>1,3</sup>✉, Xiaolin Yang<sup>1,2</sup>, Huaibao Chu<sup>1,2</sup>, Fengbin Chen<sup>1,2</sup>, Jinxing Wang<sup>1,2</sup>, Peng Guo<sup>1</sup> & Zhikai Cheng<sup>1</sup>

With the increase of the construction depth for ultra-deep shaft development blasting, it is prone to occur problems such as reduced driving efficiency, frequent dynamic disasters, wellbore instability and fracture under the coupling effect of deep high stress and strong blasting disturbance. In this paper, the dynamic evolution process of surrounding rock stress field and the propagation law of explosion stress wave in the process of ultra-deep shaft development blasting were studied by combining theoretical analysis with physical model test. The theoretical analysis model of ultra-deep shaft blasting excavation was established based on elastic mechanics, and the stress distribution and failure mechanism of surrounding rock under the coupling effect of deep high stress and blasting load were explored. Based on the self-developed dynamic response test system of surrounding rock in ultra-deep shaft development blasting, the propagation and attenuation law of blasting stress wave in surrounding rock under the influence of different ground stress characteristics were tested and analyzed. The results show that the stress distribution law of surrounding rock in ultra-deep shaft development blasting is affected by the superposition effect of the static stress field under the action of in-situ ground stress and the dynamic stress field under the action of blasting load, there is an increasing effect for the radial stress and a weakening effect for the hoop stress in the surrounding rock. There are tensile phase and compressive phase in the blasting strain waves measured in the shaft model test, and the radial direction is dominated by compressive strain, and the hoop direction is dominated by tensile strain. The blasting stress wave in the surrounding rock attenuated in the form of power exponential function with the increase of the measuring point proportional distance in the horizontal and vertical directions. The attenuation rate of the radial explosion strain wave was greater than that of the hoop strain wave. In addition, due to the influence of the propagation direction for the stress wave, the attenuation index of the radial peak strain and the hoop peak strain in the vertical direction were greater than those in the horizontal direction. The dynamic evolution process of the surrounding rock stress field and the propagation law of the explosion stress wave were further studied by experimental results compared with the theoretical analysis and the field test results in the literature. The conclusion of this study can provide a theoretical basis for the stability analysis of surrounding rock and the parameters design of development blasting in ultra-deep shaft.

**Keywords** Ultra-deep shaft, Development blasting, Superposition effect, Model test, Attenuation law of stress wave

Mining in deep mine has become one of the national deep underground strategies. At present, the mining depth of various mineral and energy resources has gradually reached 1000–2000 m, and the exploitation of deep underground resources will become the norm in the future<sup>1</sup>. As the throat project of underground mine system, the excavation depth of the shaft is constantly refreshing. According to the construction depth of the shafts, some scholars have defined shafts with a construction depth of 800–1200 m as deep shafts and those exceeding 1200 m as ultra-deep shafts. In the next 10–15 years, the construction depth of ultra-deep shaft in China is mainly concentrated in 1500–2000 m<sup>2</sup>. The geological conditions and stress environment of rock strata in the process of ultra-deep shaft construction are becoming more and more complex<sup>3</sup>, and The drilling and blasting method has become the key technology to realize the rapid excavation of ultra-deep shaft<sup>4</sup>. While the surrounding rock of

<sup>1</sup>School of Civil Engineering, Henan Polytechnic University, Jiaozuo 454000, China. <sup>2</sup>Key Laboratory of Intelligent Construction and Safety Operation and Maintenance of Underground Engineering in Henan Province, Jiaozuo 454000, China. <sup>3</sup>School of Civil Engineering, Xinyu University, Xinyu 338000, China. ✉email: bosun0419@163.com

ultra-deep shaft is prone to over-excavation or under-excavation problems and dynamic disaster effects under the combined action of deep high stress and blasting dynamic load<sup>5,6</sup>, in the process of ultra-deep shaft development blasting. It will bring a series of problems, such as increasing the instability probability of shaft surrounding rock, affecting the excavation progress and increasing the supporting cost<sup>7,8</sup>. Therefore, the dynamic evolution process of surrounding rock stress field in ultra-deep shaft development blasting must be explored, and the propagation and attenuation law of explosion stress waves in ultra-deep shaft surrounding rock also must be revealed, and it is of great significance for the stability analysis of surrounding rock and the parameters design of development blasting in ultra-deep shaft.

The coupling mechanism of deep high stress and blasting dynamic load is the key scientific problem of the application of drilling and blasting method in deep underground engineering. In recent years, researchers have carried out a lot of research on the blasting mechanism of deep rock mass from the aspects of theoretical model, experimental research and numerical simulation. Yi<sup>9</sup>, Tao<sup>10</sup> and Li<sup>11</sup> theoretically analyzed the superposition principle of the static stress field around the borehole and the dynamic stress field generated by blasting, and used the FEM method to study the influence of in-situ stress on the rock blasting. The results show that the crack propagation of the borehole and the penetration of the cracks between the holes are not only affected by the magnitude of the in-situ stress, but also affected by the lateral pressure coefficient. Under the condition of confining pressure, the width of the blasting cracks is small and the number is small. Under the influence of the lateral pressure coefficient, the crack propagation has obvious guiding effect. With the increase of the initial in-situ stress, the radius of the fracture zone decreases. He<sup>12</sup>, Peng<sup>13</sup> and Yang<sup>14</sup> carried out experimental research on the blasting failure characteristics of rock mass under different stress conditions. The experimental results show that there is an annular pre-compression stress generated by the initial confining pressure, it has an enhancement effect on the hoop compression deformation after blasting, and has a weakening effect on the tensile failure. Moreover, when the pressure direction is perpendicular to the direction of the blast hole, the damage of the specimen after blasting is large, which is not conducive to the formation of cracks. Some researchers have also further studied the propagation of explosion stress wave in deep jointed rock mass<sup>15</sup> and the superposition effect of stress wave in double-hole delayed blasting of deep rock mass<sup>16</sup>. However, these studies need to be carried out in combination with specific engineering construction.

In recent years, scholars at home and abroad have carried out research on the dynamic evolution law of surrounding rock stress in blasting excavation of deep underground caverns, which has important reference significance for the study of dynamic response characteristics of surrounding rock in ultra-deep shaft excavation blasting. Xie<sup>17</sup> used FEM software to study the damage evolution mechanism of surrounding rock by deep tunnel blasting. The results show that deep high stress hinders the extension of surrounding rock damage by explosion to a certain extent. The lateral pressure coefficient affects the extension direction of the tensile damage zone. Qiu<sup>18</sup> used the discrete element method to analyze the dynamic response characteristics of deep roadway under blasting disturbance, evaluated the influence of blasting position on blasting vibration, obtained the diffraction starting area and diffraction ending area of stress wave, and obtained the radial stress wave and tangential stress wave around deep roadway during blasting. Wang<sup>19</sup> established an analytical solution to explain the dynamic response of a deep-buried circular tunnel in unsaturated soil under axisymmetric blasting load. Hong<sup>20</sup> and Li<sup>21</sup> studied the influence of deep high stress on smooth blasting and pre-splitting blasting by numerical simulation. The study suggests that under deep high stress, it can effectively pre-crack by drilling along the principal stress direction, using less charge and uniform hole spacing. Han<sup>22</sup> used FDEM to simulate the process of rock fracture and fragmentation caused by smooth blasting during tunnel construction under deep high stress, and revealed the main influence of principal stress and lateral pressure coefficient on rock damage behavior. Since blasting excavation under deep high stress will cause transient adjustment of surrounding rock stress, the normal stress of rock mass near the excavation contour will be rapidly released and additional dynamic stress will be formed during the blasting process. Yang<sup>23</sup> used a variety of methods to study the damage disturbance mechanism of additional dynamic stress on surrounding rock under excavation transient unloading. The research showed that the magnitude of additional stress depends on the field stress level, unloading rate, excavation size and rock properties. The faster the unloading rate, the larger the excavation surface, the more obvious the damage disturbance of additional dynamic stress on surrounding rock under excavation transient unloading, and the larger the damage range in the surrounding rock. Zhang<sup>24</sup> comprehensively analyzed the distribution of blasting vibration velocity on the side wall of deep underground caverns, and gave the mechanical analysis model of the side wall of deep underground caverns and the peak particle velocity prediction formula of surrounding rock for caverns considering ground stress. The research showed that there is an amplification effect of peak particle velocity in the middle of the side wall of underground caverns, and the peak particle velocity on the side wall increases with the increase of ground stress and lateral pressure coefficient.

Due to the particularity of shaft excavation, the dynamic response induced by ultra-deep shaft development blasting is affected by unique spatial geometry and constraints. The dynamic response characteristics of shaft development blasting are different from those of deep underground cavern blasting. Zhang<sup>8</sup> studied the strength deterioration effect of fresh concrete lining for a shaft caused by blasting vibration, and proposed that the appropriate blasting time and additives to transform the negative effects caused by blasting vibration into positive effects. Zhao<sup>25</sup> simulated the excavation process of a shaft by selecting different radial stress coefficients, and expounded the disturbance stress response mechanism of surrounding rock in cross section and longitudinal section of a shaft based on the redistribution of excavation disturbance stress and the failure evolution process of surrounding rock. Shan<sup>26,27</sup> measured the stress and deformation of the concrete shaft wall under the action of millisecond blasting through similar simulation tests. The attenuation formulas of axial stress and tangential stress peaks were obtained by using similar Sadoy's formula. The signal vibration energy attenuation influence of elevation difference and equivalent distance was analyzed from the perspective of energy distribution characteristics, and the energy prediction formula was established by dimensional analysis. Hu<sup>28</sup> concluded

that excavation unloading is the main cause of micro-cracking in the surrounding rock, and that MS activity increases with the depth of vertical shafts. Xie<sup>29</sup> obtained the distribution law of dynamic strain rate induced inside the perimeter rock of vertical shafts blasting excavation through field test, the peak strain rate decreases with the increase of proportional distance, and the higher the rock strength the stronger the dynamic response. Li<sup>30</sup> found the elevation amplification effect of blasting vibration in the vertical shaft while the blasting vibration monitoring was carried out in the outlet shaft of Xiluodu hydroelectric power station, and put forward the formula of blasting vibration velocity attenuation considering the elevation factor. Zuo<sup>31</sup> proposed deep-hole segmental trench blasting of vertical shaft and a damage control scheme with peripheral directional fracture by combining indoor and field tests, which not only enhanced the efficiency of vertical shaft digging, but also reduced the damage of the explosion to the surrounding rock.

To summarize, the existing research mainly focus on the blasting mechanism of deep rock mass and the dynamic response of surrounding rock in deep-buried cavern blasting. Although some scholars have achieved in evolution law of stress field and propagation characteristics of vibration wave in the process of shaft development blasting. However, the research methods were mainly based on numerical simulation and on-site monitoring, and there are some problems for on-site testing, with difficulty in measuring point layout and large dispersion of test data. In addition, compared with the dynamic response characteristics of surrounding rock during shallow shaft development blasting, there are few studies on the dynamic response characteristics of surrounding rock at different excavation depths. Due to the importance of understanding the dynamic evolution process of surrounding rock stress field during the development blasting of ultra-deep shaft, and the significant influence of the propagation law of explosion stress wave on the surrounding rock stability of vertical shafts, a theoretical analysis model of development blasting of ultra-deep shaft was established in this study, and the surrounding rock stress distribution and failure mechanism of shaft under the action of deep high stress and blasting load were explored. Then, a self-developing test system for dynamic response model of surrounding rock for ultra-deep shaft during development blasting was developed, and the rationality of using high-pressure gas as dynamic load source was discussed. Finally, a test scheme with excavation depth and dynamic load strength as variables was designed. The propagation and attenuation law of explosion stress wave in horizontal and vertical directions of shaft surrounding rock were analyzed in detail. It provides a theoretical basis for the stability analysis of surrounding rock and the parameters design of development blasting in ultra-deep shaft.

## Theoretical analysis of stress distribution of surrounding rock in ultra-deep shaft development blasting

### Engineering background

This study takes the ultra-deep shaft under construction in a gold mine in Shandong Province as the engineering background. The wellhead elevation is +15 m, the bottom elevation is −1990 m, the shaft depth is 2005 m, and the shaft bedrock section is excavated by full-face drilling and blasting method, the net diameter of the shaft section is Φ10.5 m, and the diameter of the excavation section is Φ11.5 m, which belongs to the large-diameter ultra-deep shaft.

According to the distribution law of ground stress tested by hydraulic fracturing method<sup>32</sup>, the ground stress in the shaft area increases linearly with the increase of buried depth. The maximum horizontal principal stress at the buried depth of 2000 m reaches 60–70 MPa, and the direction of the maximum horizontal principal stress is NWW-SEE or near EW direction. The ground stress state is mainly horizontal tectonic stress, and the stress distribution law is shown in Formula (1). Where  $\sigma_H/\sigma_V$  and  $\sigma_h/\sigma_V$  gradually decrease with the increase of buried depth and finally tend to be stable. When the buried depth is deeper than 1000 m,  $\sigma_H/\sigma_V$  is basically stable between 1.0 and 1.5,  $\sigma_h/\sigma_V$  is about 1.0,  $\sigma_H/\sigma_h$  is about 1.25–1.5. According to the results of comprehensive geological exploration<sup>32,33</sup>, the lithology is mainly monzonitic granite, sericitized granite and a small amount of lamprophyre, potassic granite and greisen. The uniaxial compressive strength (UCS) of the surrounding rock is from 124 to 157 MPa, and the elastic modulus range is from 39.1 to 55.6 GPa, which belongs to a typical hard rock shaft.

$$\begin{cases} \sigma_H = 0.030H + 10.142 & R^2 = 0.9753 \\ \sigma_h = 0.019H + 7.986 & R^2 = 0.9815 \\ \sigma_V = 0.027H - 0.019 & R^2 = 0.9995 \end{cases} \quad (1)$$

where  $\sigma_H$ ,  $\sigma_h$ ,  $\sigma_V$  are the maximum horizontal principal stress, the minimum horizontal principal stress and the vertical principal stress respectively, MPa;  $H$  is the depth, m;  $R$  is the correlation coefficient.

According to a large number of in-situ stress test results and the distribution law of ground stress in the shaft construction area, the in-situ stress state of rock mass shows non-uniformity<sup>1</sup>. Therefore, the effects of uniform and non-uniform stress fields on the dynamic behavior of rock during blasting were investigated in this paper. As shown in Table 1, under the condition of uniform ground stress,  $\sigma_H = 15$  MPa, 30 MPa, 45 MPa, 60 MPa were taken to analyze the static stress distribution of surrounding rock under different ground stress levels (corresponding to different excavation depths). Under the condition of non-uniform ground stress, keeping  $\sigma_H = 40$  MPa (the maximum horizontal principal stress at the excavation depth  $H = 1000$  m is calculated according to Formula (1)), five sets of non-uniformity coefficients were determined, which are set to 0, 0.25, 0.5, 0.75 and 1.0 respectively, and the influence of ground stress anisotropy on the static stress distribution law of surrounding rock was analyzed.

Combined with the shaft surrounding rock conditions, a blasting chart suitable for the excavation of ultra-deep shaft was designed though the technologies with the smooth surface, smooth bottom, weak shock, weak impact and medium-deep hole blasting. The specific blast hole layout is shown in Fig. 1. Seven circles of blasting holes were arranged from the inside to outside on the excavation face. The smooth blasting method of straight

Buried depth H/m	$\sigma_h$ /MPa	$\sigma_H$ /MPa	$\frac{\sigma_h + \sigma_H}{2}$ /MPa	Buried depth H/m	Non-uniform coefficient $k$	$\sigma_h$ /MPa	$\sigma_H$ /MPa
500	17.5	25.1	21.3	1000	0	0	40
1000	27	40.1	33.6	1000	0.25	10	40
1500	36.5	55.1	45.8	1000	0.5	20	40
2000	46	70.1	58.1	1000	0.75	30	40

**Table 1.** In-situ stress conditions in this study.

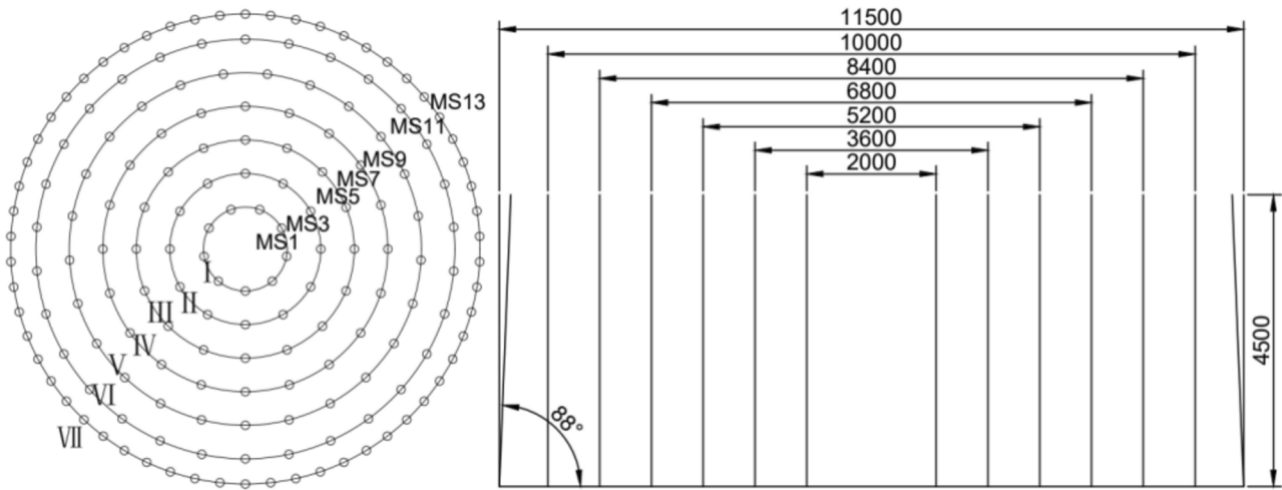


**Fig. 1.** Layout of the blasting bores in shaft construction by full-face drilling and blasting method (unit: mm).

hole cutting and segmented delay was adopted. The half-second delay electronic detonator was detonated in turn with seven sections according to the order of MS1, MS3, MS5, MS7, MS9, MS11 and MS13. To achieve the best blasting effect, the blasting parameters will be adjusted in time according to the actual geological conditions during the construction process.

**Theoretical analysis model**

In the process of ultra-deep shaft development blasting, with the blasting of the blasted rock mass, the internal stress of the surrounding rock is redistributed under the influence of ground stress, and a dynamic stress field will be formed in the shaft surrounding rock with the propagation of the explosion stress wave<sup>34</sup>. The stress in deep rock mass under blasting can be regarded as the superposition of deep high stress and blasting load. After blasting, the crushing zone, fracture zone and elastic vibration zone are formed around the blast hole in turn. Since the ground stress in the rock mass is much smaller than the shock wave pressure caused by blasting, so there is little effect of the ground stress on the formation of the crushing zone. However, as the shock wave gradually decays into a stress wave, ground stress and stress wave play an important role in the formation of the fracture zone. Specifically, the coupling of stress wave and ground stress produces hoop tensile stress in the rock mass, which affects the propagation of radial cracks and directly affects the blasting effect. Therefore, it is very important to analyze the influence of ground stress on the propagation of blasting stress wave. According to the distribution law of ground stress in shaft construction area and the characteristics of blasting load caused by different blastholes (cut holes, easer holes and contour holes), combined with elastic–plastic mechanics and stress wave theory, the theoretical analysis model of ultra-deep shaft blasting excavation is simplified, and the following assumptions are made:

1. It is assumed that the surrounding rock of the shaft is isotropic, homogeneous and continuous elastic medium. The overall stress state of the shaft as shown in Fig. 2a.
2. Because the length of the borehole is much larger than its diameter, and the main direction length of the shaft is much larger than the section radius, the blasting problem of the shaft surrounding rock under the influence of the ground stress can be simplified as the elastic dynamic problem under the condition of plane strain, as shown in Fig. 2b. The elastic dynamic behavior of the surrounding rock is obtained by superimposing the static stress distribution caused by the in-situ stress field and the dynamic response caused by the blasting load.
3. The surrounding rock of the shaft is subjected to the maximum horizontal principal stress  $\sigma_H$  and the minimum horizontal principal stress  $\sigma_h$  in the far field, as shown in Fig. 2c, and its size can be determined according to the distribution law of ground stress.

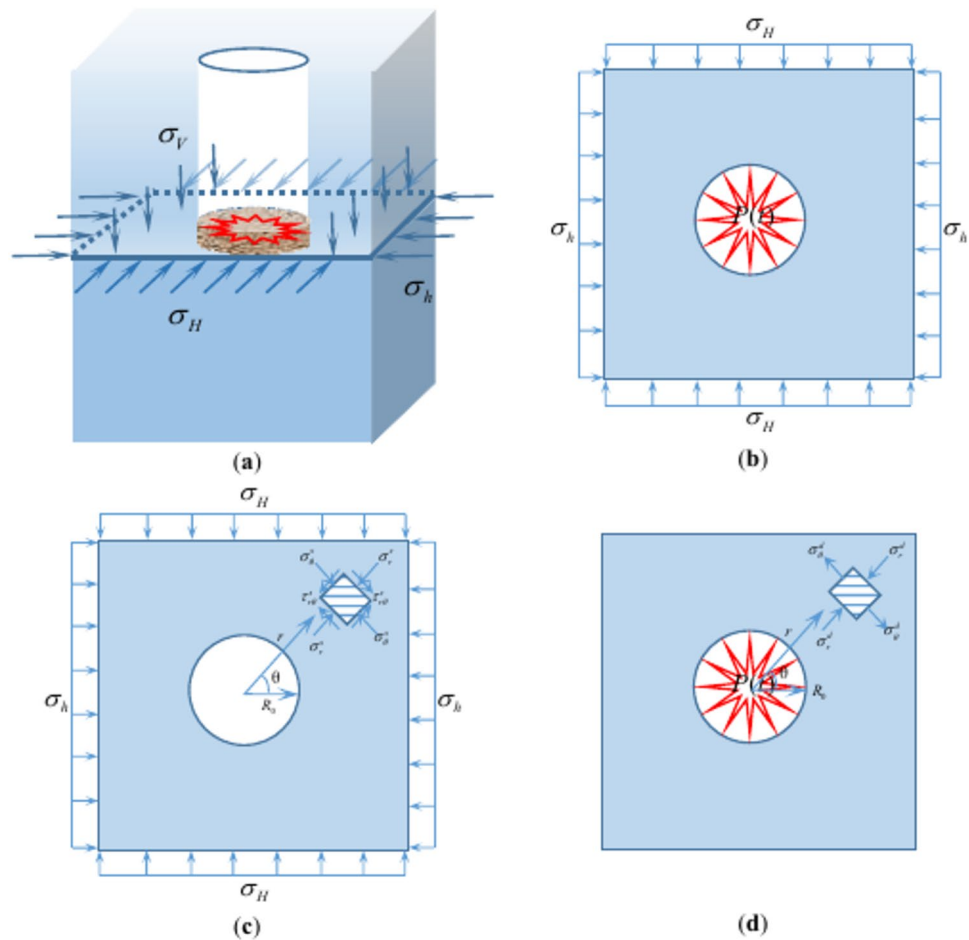


**Fig. 2.** Geometric models for theoretical analysis: (a) The overall stress state of the shaft; (b) Elastic dynamic problems under plane strain condition; (c) Stress analysis under static load; (d) Stress analysis under dynamic load.

- It is assumed that the blasting pressure generated by development blasting is approximately evenly distributed, and the stress field in the middle-far zone in the blasting of the shaft surrounding rock is treated as elastic stress. The blasting load  $P(t)$  generated by the simultaneous initiation of boreholes can be reduction calculated according to the blasting load on the wall of single-hole blasting, and then applied to the excavation boundary. As shown in Fig. 2d.

#### Static stress field of surrounding rock under ground stress

According to the layout of blasting bores in shaft construction by full-face drilling and blasting method, the explosion cavity will be formed after each circle of blastholes in the shaft are detonated in turn, which will also cause the redistribution of ground stress. The size of the explosion cavity is related to the type of blastholes (Cut holes, Easer holes, Contour holes), which is expressed as  $R_0$  here. As shown in Fig. 2c, a small unit at the distance from the center of the shaft  $r$  is taken as the analysis object of the mechanical model. A polar coordinate system is established with the center of the shaft as the origin, and the direction of the compressive stress is defined as the positive direction of the stress. Based on the theory of elastic mechanics, the analytical formula of static stress distribution of surrounding rock under far-field stress is obtained:

$$\begin{cases} \sigma_r^s = \left( \frac{\sigma_h + \sigma_H}{2} \right) \left( 1 - \frac{R_0^2}{r^2} \right) + \left( \frac{\sigma_h - \sigma_H}{2} \right) \left( 1 - \frac{R_0^2}{r^2} \right) \left( 1 - 3 \frac{R_0^2}{r^2} \right) \cos 2\theta \\ \sigma_\theta^s = \left( \frac{\sigma_h + \sigma_H}{2} \right) \left( 1 + \frac{R_0^2}{r^2} \right) - \left( \frac{\sigma_h - \sigma_H}{2} \right) \left( 1 + 3 \frac{R_0^4}{r^4} \right) \cos 2\theta \\ \tau_{r\theta}^s = \left( \frac{\sigma_H - \sigma_h}{2} \right) \left( 1 - \frac{R_0^2}{r^2} \right) \left( 1 + 3 \frac{R_0^2}{r^2} \right) \sin 2\theta \end{cases} \quad (2)$$

where  $\sigma_r^s$ ,  $\sigma_\theta^s$ ,  $\tau_{r\theta}^s$  are radial stress, hoop stress and shear stress, respectively, MPa; the superscript  $s$  indicates the case of static loading. The  $r$  and  $\theta$  are the distance and direction angles relative to the shaft center, respectively.



According to the analytical calculation formula (2), the stress distribution on the boundary of the blasting cavity and the change process of the surrounding rock stress with the increase of the distance from the center of the shaft can be determined. However, when  $r = R_0$ , that is  $\sigma_r^s = \tau_r^s = 0$ , under the action of uniform stress field and non-uniform stress field, the radial stress and shear stress on the boundary of blasting cavity are always 0. Therefore, the boundary position of the blasting cavity is in the state of free surface, and the hoop stress distribution on the boundary of the blasting cavity can represent its stress distribution state. The hoop stress distribution on the boundary ( $r = R_0$ ) of the blasting cavity and the variation of the surrounding rock stress with the increase of the distance from the center of the shaft under the condition of uniform stress can be shown in Fig. 3a,b. The distribution of hoop stress on the boundary of blasting cavity under the condition of non-uniform stress can be shown in Fig. 4a. The distribution of hoop stress, radial stress and shear stress in the middle-far zone ( $r = 8R_0$ ) of blasting can be shown respectively in Fig. 4b–d. The variation law of surrounding rock stress in horizontal and vertical directions with the increase of distance from the center of shaft can be shown respectively in Fig. 4e,f, where the positive value of stress represents compressive stress and the negative value represents tensile stress.

From Fig. 3a, it can be seen that under the action of uniform stress field, the hoop stress on the boundary of blasting cavity is axisymmetric compressive stress distribution along all directions, and the magnitude of hoop stress increases with the increase of hydrostatic pressure, which is 2 times of the initial stress. This shows that in the uniform stress field, the stress concentration phenomenon is easy to occur near the blasting excavation boundary, which increases with the increase of the initial ground stress. Therefore, the blasting damage and fracture will be limited to the same extent in all directions, and the higher the initial ground stress, the stronger the limiting effect. In addition, as shown in Fig. 3b, with the increase of the distance from the shaft center, the hoop stress decreases and the radial stress increases, and finally gradually approaches the initial ground stress value under various conditions. Although the stress concentration effect of surrounding rock stress is gradually weakened, the limiting effect of blasting damage is still increasing with the increase of initial ground stress.

Therefore, it can be concluded that it plays a key role for ground stress in the dynamic response of rock under the action of blasting load, mainly by changing the stress path to promote the dynamic compaction of rock and reduce the explosive fracture caused by the superposition effect of surrounding compression.

Although the edge of the blasting cavity is not affected by radial stress and shear stress under the action of non-uniform stress field, the hoop stress distribution no longer exhibits axisymmetric characteristics. As shown in Fig. 4a, the loading stress  $\sigma_H$  in the vertical direction remains unchanged. As the loading stress  $\sigma_h$  in the horizontal direction gradually increases (or as the stress non-uniformity coefficient  $k$  continues to increase), the hoop stress distribution in different directions at the edge of the blasting cavity is significantly different, and two different extreme values appear in the initial stress loading direction. The maximum hoop stress is located in the horizontal direction of the action  $\sigma_h$ , and decreases with the increase of  $k$ . However, the minimum hoop stress is located in the vertical direction of the action  $\sigma_H$ , and increases with the increase of  $k$ . The increase rate of the minimum hoop stress is more significant than the decrease rate of the maximum hoop stress. That is, as the stress non-uniformity coefficient  $k$  continues to approach 1, the stress concentration effect of the surrounding rock stress field gradually weakens. In addition, when the lateral pressure coefficient  $k = 0$  is used, the compressive stress and tensile stress concentration appear at the edge of the blasting cavity in the horizontal and vertical directions, respectively. Considering the tensile/compressive strength characteristics of the rock mass, the rock

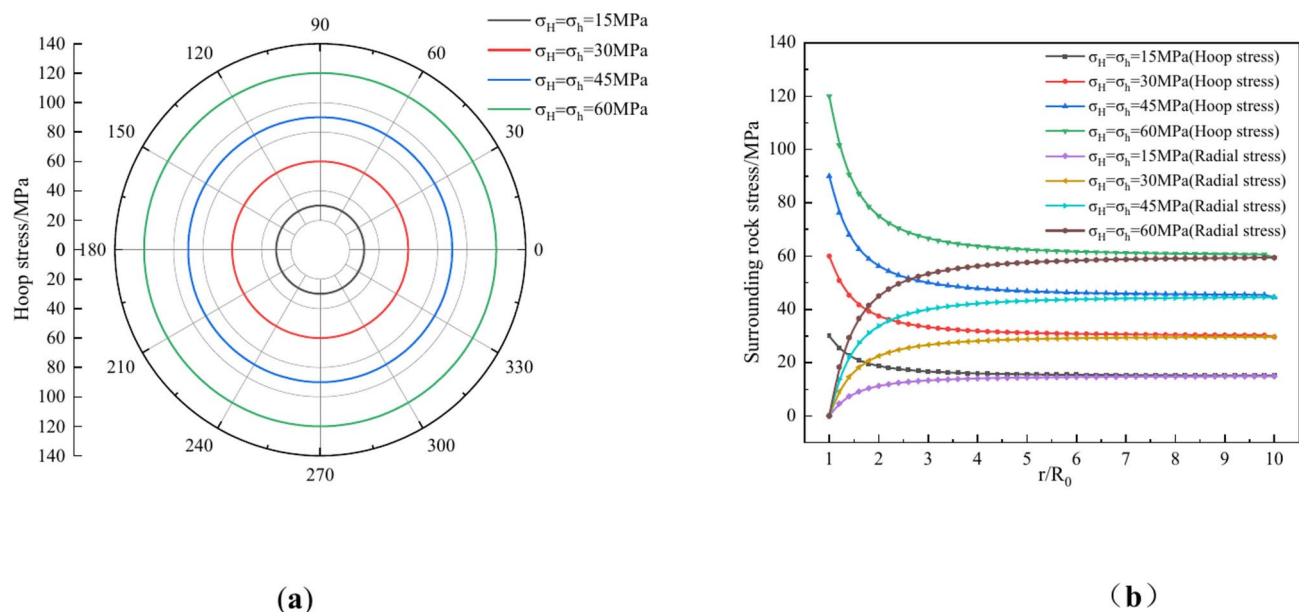


**Fig. 3.** Static stress distribution law of surrounding rock under uniform stress: (a) Hoop stress distribution for  $r = R_0$ ; (b) Surrounding stress variation of at different distances under static load (hoop stress/radial stress).

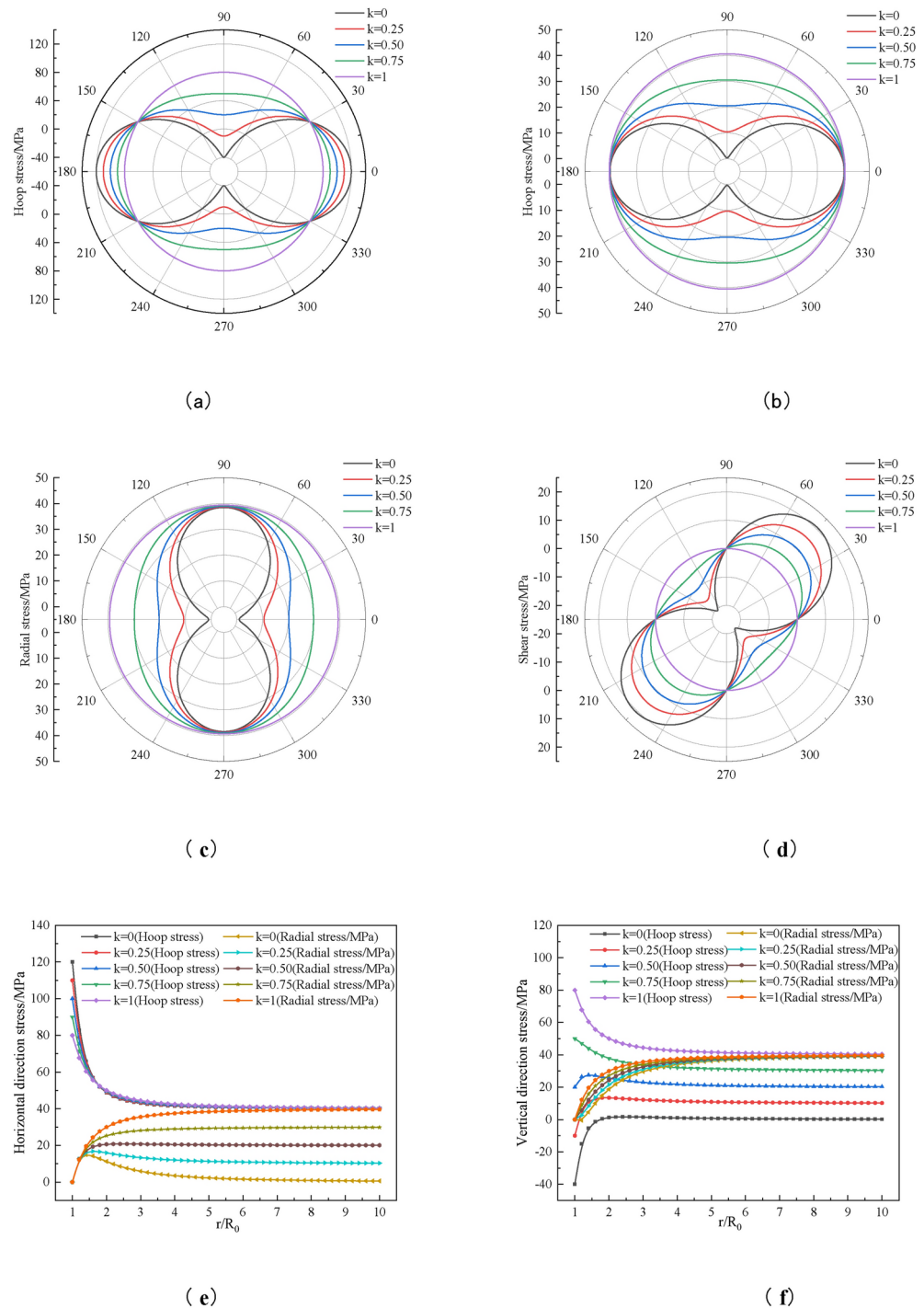


**Fig. 4.** Static stress distribution law of surrounding rock under non-uniform stress: (a) Hoop stress distribution for  $r = R_0$ ; (b) Hoop stress distribution for  $r = 8R_0$ ; (c) Radial stress distribution for  $r = 8R_0$ ; (d) Shear stress distribution for  $r = 8R_0$ ; (e) Surrounding stress variation of in the horizontal direction under static load; (f) Surrounding stress variation of in the vertical direction under static load.

mass failure at the initial tensile stress will be more serious. According to the variation law of hoop stress, the critical lateral pressure coefficient  $k = 1/3$  for the transformation of tensile stress into compressive stress can be determined.

The stress concentration effect of surrounding rock in the near area of blasting is obvious. The stress distribution characteristics of surrounding rock in the middle-far area of blasting was further analyzed in this paper. As shown in Fig. 4b, at a long distance from the center of the shaft, the maximum hoop stress is located in the horizontal direction of the action  $\sigma_h$ , and its size is not affected by the stress non-uniformity coefficient, which is consistent with the loading stress  $\sigma_H$  in the vertical direction. The minimum hoop stress is located in

the vertical direction of the action  $\sigma_H$ , and increases with the increase of  $k$ , but its increase rate is weaker than that of the near blasting area. As shown in Fig. 4c, the radial stress at a long distance from the center of the shaft is similar to the hoop stress distribution law, and only a 90° deflection occurs in the direction, that is, the maximum radial stress value in the vertical direction is independent of the stress non-uniformity coefficient, and the minimum radial stress value in the horizontal direction increases with the increase of  $k$ . As shown in Fig. 4d, the change of shear stress in the middle-far zone of blasting shows obvious quadrant difference. The shear stress is 0 in both horizontal and vertical directions, compressive stress in 1 and 3 quadrants, tensile stress in 2 and 4 quadrants, and the shear stress always reaches the peak in the center of each quadrant, which decreases with the increase of stress non-uniformity coefficient  $k$ .

The stress change process at different positions from the shaft center in the horizontal and vertical directions under the action of non-uniform stress field can be shown in Fig. 4e,f show, respectively. The stress in the horizontal and vertical directions gradually tends to be stable with the increase of distance. The stress concentration effect of surrounding rock decreases rapidly in the range of  $R_0 : 3R_0$ , and the stress concentration effect of surrounding rock is basically stable in the range of  $3R_0 : 10R_0$ . In addition, in two directions, the relative values of radial stress and hoop stress change with the lateral pressure coefficient, and the horizontal direction stress is dominated by hoop stress, and the vertical direction stress is dominated by radial stress. It is generally believed that hoop stress is the key factor causing radial cracks. Under the action of non-uniform stress field in different directions, the development of radial cracks shows a certain degree of directional change, which means that the trend of crack growth is more inclined to the direction of maximum initial stress. In addition, with the increase of the initial stress difference in the horizontal and vertical directions, the propagation of radial cracks is more significant in terms of anisotropy.

### Dynamic stress field of surrounding rock under blasting load

A large number of high-temperature and high-pressure detonation products will be produced in a short time after the detonation of explosives in the blasthole, and complex interactions will occur with the hole wall. The initial shock wave will be formed on the hole wall, causing the rock mass near the blasthole to be excessively broken to form a crushing zone. At the same time, the shock wave will rapidly decay into a stress wave and continue to propagate to the surrounding rock mass medium. Therefore, the dynamic stress field of surrounding rock under blasting load is directly related to the blasting load generated by explosive detonation.

Under the condition of coupling charge, the impact load is applied to the rock after the charge blasting. According to the C-J detonation theory of the condensed explosive detonation wave and the acoustic approximation principle, the blasting load on the borehole wall can be calculated by Formula (3)<sup>35</sup>:

$$P_0 = \frac{\rho_e D_e^2}{\gamma + 1} \cdot \frac{2\rho_r C_p}{\rho_r C_p + \rho_e D_e} \quad (3)$$

where  $P_0$  is the blasting load on the borehole wall, MPa;  $\rho_r$  and  $\rho_e$  are the density of rock and explosive, kg/m<sup>3</sup>, respectively;  $C_p$  and  $D_e$  are the longitudinal wave velocity of rock and the detonation velocity of explosive, respectively, m/s;  $\gamma$  is the expansion adiabatic index of detonation products, it is generally approximately 3 for most explosives.

Under the condition of uncoupled charge, according to the multi-party gas state equation, the blasting load on the borehole wall can be calculated by Formula (4)<sup>35</sup>:

$$P_0 = n \frac{\rho_e D_e^2}{2(\gamma + 1)} K_d^{-2\gamma} K_l^\gamma \quad (4)$$

where  $K_d$  is the radial uncoupling coefficient of the charge,  $K_d = d_b/d_c$ ,  $d_b$  and  $d_c$  are the diameter of the blast hole and the diameter of the cartridge, mm, respectively;  $K_l$  is the axial charge coefficient,  $K_l = l_c/l_b$ ,  $l_c$  and  $l_b$  are the total length of the grain and the length of the hole charge section, mm, respectively;  $n$  is the pressure increase coefficient when the explosive detonation product expands and hits the hole wall,  $n = 8 \sim 11$  and it is generally 10.

It can be seen from Fig. 1 that the blasting excavation process of the shaft involves the simultaneous initiation of multiple blast holes. The dynamic stress field of the shaft surrounding rock is not only related to the charge structure of the blast hole, but also related to the arrangement of the blast holes on the excavation boundary. Therefore, the blasting load on the blasting excavation boundary of each section can be determined according to the equivalent blasting load.

For cut blasting (MS1 section), it is necessary to reduce the blasting load on the wall of a single blast hole according to the attenuation law of stress wave and apply it to the excavation surface equivalently. The blasting load on the equivalent elastic boundary can be calculated by formula (5)<sup>36</sup>:

$$P_b = kP_0 \left( \frac{r_c}{r_b} \right)^{-\alpha_1} \left( \frac{r_f}{r_c} \right)^{-\alpha_2} \quad (5)$$

where  $P_b$  and  $P_0$  are the blasting load on the excavation surface of the cutting section and on the wall of a single borehole, MPa, respectively;  $k$  is an influence factor of multiple blastholes, which is related to the number and arrangement of blastholes;  $r_b$ ,  $r_c$  and  $r_f$  are the radius of a single borehole, the radius of the crushing zone and the radius of the fracture zone;  $\alpha_1$  and  $\alpha_2$  are impact attenuation index and stress wave attenuation index, respectively,  $\alpha_1 \approx 3.0$  or  $\alpha_1 = 2 + \mu_d/(1 - \mu_d)$  for shock wave,  $\alpha_2 = 2 - \mu_d/(1 - \mu_d)$  for stress wave;  $\mu_d$



is the dynamic Poisson's ratio of rock. In the range of engineering blasting loading rate,  $\mu_d = 0.8\mu_0$  and  $\mu_0$  is the static Poisson's ratio of rock.

For the blasting of auxiliary holes and peripheral holes (MS3, MS5, MS7, MS9, MS11 and MS13 section), the blasting load on all the blasthole walls in the same section is averaged to the excavation boundary determined by the line connecting the center of the whole blasthole and the axis of the blasthole. According to the Saint-Venant principle, the equivalent load on the excavation surface can be calculated by Formula (6)<sup>36</sup>:

$$P_b = P_0 \frac{2r_b}{S} \quad (6)$$

where  $S$  is the distance between two adjacent holes.

As the blasting load in the surrounding rock continues to propagate outward, its strength continues to decay, and finally it becomes an elastic-plastic stress wave. The radial stress and hoop stress at any point in the surrounding rock of the shaft can be expressed by formulas (7) and (8) respectively<sup>35</sup>:

$$\sigma_r^d = P_b (r/R_0)^{-\alpha} \quad (7)$$

$$\sigma_\theta^d = -\lambda \sigma_r^d \quad (8)$$

where  $\sigma_r^d$  and  $\sigma_\theta^d$  are the radial stress and hoop stress in the shaft surrounding rock during the blasting for each section of the blast hole, MPa, and the superscript  $d$  indicates the dynamic loading situation;  $\alpha$  is the stress wave attenuation index;  $\lambda$  is the dynamic lateral pressure coefficient,  $\lambda = \mu_d / (1 - \mu_d)$ .

### Superimposed stress field of blasting load and ground stress

Due to the different distance between the excavation boundary of each blasting hole and the shaft, the formula (3)–(6) can be brought into the formula (7) and the formula (8) respectively, and the distribution law of the dynamic stress field of the shaft surrounding rock is obtained considering comprehensively the charge structure and the initiation of different blasting holes. Combined with the theoretical results of the mechanism of deep rock mass blasting action<sup>10,11</sup>, by using the superposition principle, the radial stress  $\sigma_r$  and hoop stress  $\sigma_\theta$  at any point in the shaft surrounding rock under the combined action of ground stress and blasting load are obtained respectively:

$$\sigma_r = \sigma_r^s + \sigma_r^d \quad (9)$$

$$\sigma_\theta = \sigma_\theta^s + \sigma_\theta^d \quad (10)$$

Because the blasting load and the static stress field caused by the redistribution of ground stress are different in the millisecond blasting for each section of the shaft, Formula (9) and Formula (10) can be used as the general formula of the superimposed stress field. In order to intuitively reflect the superposition effect, Chen<sup>37</sup> conducted a comprehensive analysis of the stress characteristics around the blasting hole, as shown in Fig. 5.

During the whole blasting process, due to the existence of in-situ ground stress, the distribution of radial stress and hoop stress in surrounding rock is not uniform, and there are different effects for the in-situ stress on the dynamic load generated by blasting at different positions, since the direction of radial stress generated by blasting load and in-situ stress is the same, so they play a superposition role. The medium around the fracture hole bears a large compressive stress. The blasting load is opposite to the tangential stress generated by the in-situ stress, thus they offsetting each other. However, considering the blasting load is huge and decays rapidly, the tensile stress near the fracture area is applied. As the distance increases, the tensile stress gradually decreases and gradually transforms into compressive stress. When the lateral pressure coefficient is 0, the rock mass around the borehole is in a uniaxial stress state, and there will be shear stress in the direction of 45° above the borehole. Therefore, the comprehensive influence of blasting load and ground stress must be considered in the analysis of rock mass stress.

Because the rock belongs to the typical brittle material, it has the characteristics of good compression resistance and poor tensile resistance, so it can be considered that the damage of the rock in the middle-far area of the blasting is mainly controlled by the hoop stress. When  $\sigma_\theta \geq \sigma_{td}$ , the radial cracks will occur. It can be seen from Formula (9) that the existence of ground stress will weaken the hoop stress generated by the propagation of explosion stress wave. After the superposition of the compressive stress generated by the in-situ stress in the middle-far zone of the blasting and the hoop tensile stress induced by the blasting load, it is possible that the superimposed tangential tensile stress is less than the dynamic tensile strength of the rock, thereby inhibiting the expansion of the blasting crack, reducing the effective cracking range of the blasting, and effectively reducing the blasting damage range at the excavation boundary of the shaft.

### Physical model test design

The coupling effect of blasting excavation dynamic disturbance stress and deep high stress is the fundamental driving force of deformation and failure of surrounding rock in ultra-deep shaft. Therefore, the study of stress distribution and evolution of surrounding rock in shaft during blasting excavation is the basis of stability analysis and control of surrounding rock. Although on-site monitoring is the most direct and effective method to obtain the mining stress of surrounding rock for shaft development blasting<sup>29,30</sup>, but it is often limited by the test environment and test methods, the test data obtained is limited and discrete. Therefore, in order to better reveal the dynamic response law of blasting excavation to the surrounding rock of ultra-deep shaft, the indoor blasting

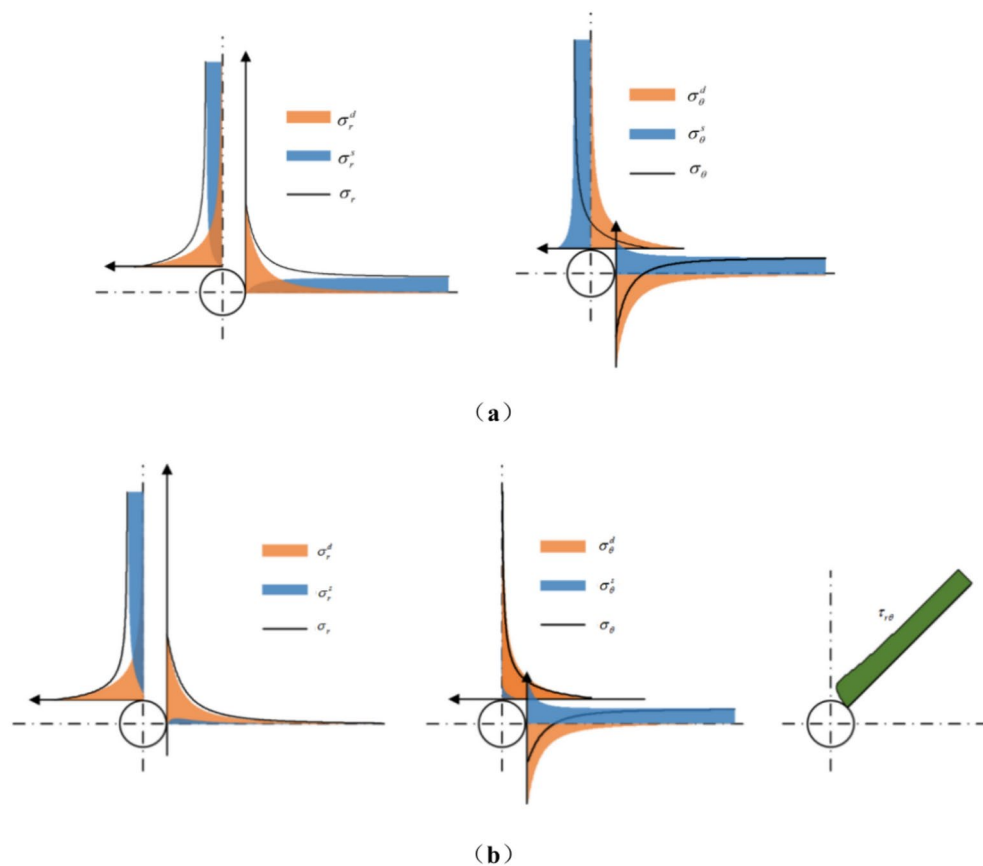


**Fig. 5.** Stress superposition effect around blasting hole<sup>37</sup>: (a) Uniform stress state,  $k=1$ ; (b) Non-uniform stress state,  $k=0$ .

model test has become an effective research method to obtain the disturbance stress distribution of surrounding rock<sup>26,27</sup>. Based on the similarity theory, this method realizes the similarity between the physical properties of the model material and the field engineering prototype, and the boundary conditions are as similar as possible to the field conditions. The results of similar model test visually reproduce or predict the dynamic response of surrounding rock caused by blasting disturbance under specific geological conditions.

### Research and development of model test system

To analyze the dynamic response characteristics of surrounding rock of ultra-deep shaft development blasting, we developed a physical model test system with combined loading function of three-dimensional static stress and explosion shock. The test system is mainly composed of four parts, including true triaxial static loading system, high-pressure gas pressurization system, high-pressure gas explosion shock control system and data acquisition and processing system. The maximum model sample size of the model test system is 500 mm × 500 mm × 500 mm. Three-way synchronous loading can be realized by the true triaxial static loading system, and the load range is from 0 to 300 kN. The peak pressure range generated by the high-pressure gas blasting impact system is from 0.1 to 80 MPa. The data acquisition and processing system includes the hole wall pressure test subsystem, the surrounding rock explosion strain test subsystem, surrounding rock vibration test subsystem and so on. During the test, the model was subjected to three-dimensional static loading through the hydraulic loading control system, and it can simulate the boundary conditions of shafts at different depths, and different blasting loads can be applied through the gas pressurization system and release control system. The DH8302 and DH5922D portable dynamic signal test and analysis systems can be used to realize the real-time acquisition of dynamic physical quantities such as hole wall blasting load, strain and vibration acceleration inside the surrounding rock. The details as shown in Fig. 6.

In this experiment, the high-pressure gas blasting impact system was used as the device to apply the blasting load. It is the key to ensure that the hole wall pressure generated by the high-pressure gas impact has a certain similarity with the blasting. According to the previous exploratory research on the mechanism of coal blasting under the impact of high-pressure gas<sup>38,39</sup>, the hole wall peak pressure of high-pressure gas blasting is proportional to the impact pressure, the pressure rise time is about 100ms, and the loading rate can reach 1GPa/s. The waveform of high-pressure gas blasting stress wave has compressive phase and tensile phase which is similar to that of explosive explosion stress wave. The radial direction is dominated by compressive stress wave, and the hoop direction is dominated by tensile stress wave. It can be seen that the load generated by high-

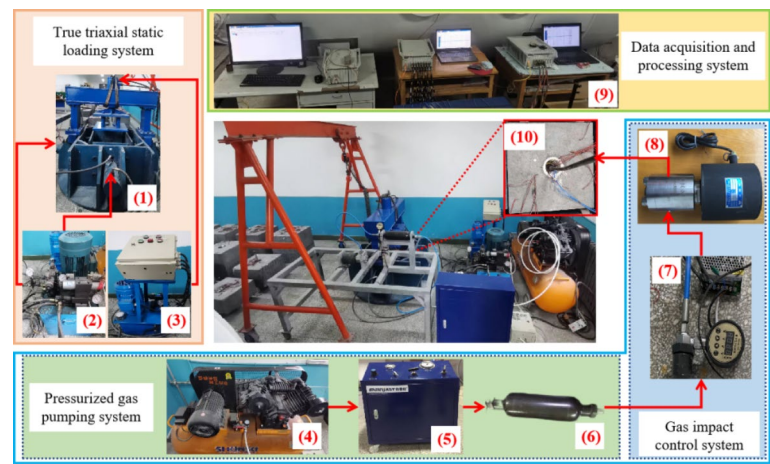


**Fig. 6.** Model test system: (1) True triaxial static loading device; (2) Horizontal hydraulic pump station; (3) Vertical direction hydraulic pump station; (4) Air compressor; (5) Booster pump; (6) Pressure kettle; (7) CNC pressure gauge; (8) Solenoid valve; (9) Data acquisition device; (10) Model sample.

Material	Density/(g/cm <sup>3</sup> )	Compressive strength/MPa	Tensile strength/MPa	Elastic modulus/GPa	Poisson ratio	Cohesion/MPa	Angle of internal friction/°
Prototype rock <sup>32,33</sup>	2.63	153.7	11.7	41.4	0.21	24.89	55.5
Model material	2.51	3.50	0.30	0.85	0.22	0.50	44.8

**Table 2.** Physical and mechanical parameters of prototype rock and model materials.

pressure gas blasting impact belongs to strong pressure pulse load, which conforms to the characteristics of blasting load. Thus high-pressure gas blasting can be used as an alternative method of explosive blasting in the laboratory, and it can also solve the problem that the ordinary laboratory cannot purchase and carry out blasting dynamic load test due to explosive control.

**Determination of similar proportion and similar material**

According to the theory of rock mechanics and similarity theory<sup>40</sup>, the similarity ratio of qualitative variables is generally set to 100–200, while the similarity ratio of quantitative variables is generally 20–50. There is a great influence for geometric similarity ratio in the model test on the rationality of the actual engineering simulation. Based on the engineering background of this paper, the geometric similarity ratio of the proposed model was 1:100, the material bulk density similarity ratio was 1:1, and the elastic modulus and stress similarity ratio were 1:100. The similarity ratio of other dimensionless physical quantities including strain, internal friction angle, Poisson’s ratio, friction coefficient and other physical quantities was 1:1. According to the existing model test experience<sup>41</sup>, when the model size is 3–5 times of the excavation tunnel, the test error meets the engineering requirements. The shaft test model is usually designed as a circle. However, considering the problems of shaft production, test element installation and initial ground stress application, the model size was designed as 500 mm × 500 mm × 460 mm (L × W × H), and the internal shaft size was Φ110 mm × 260 mm (D<sub>1</sub> × h<sub>1</sub>). The determination of shaft size takes into account the height of six development blasting cycles in actual construction and the working gap between the wellbore and the heading face. The single hole size of Φ25 mm × 100 mm (D<sub>2</sub> × h<sub>2</sub>) was designed to simulate the cut blasting in Fig. 1, and its size meets the geometric similarity ratio. The resistance line at the bottom of the blast hole was 100 mm.

The selection of similar materials is one of the key factors for the success of physical simulation experiments<sup>42,43</sup>. The selected similar materials were composed of quartz sand (20–40 mesh), iron powder (80–150 mesh), barite powder (325 mesh), cement (P.O32.5) and water. After several trials, the optimal mix ratio of similar materials to meet the requirements of ultra-deep shaft blasting model test was obtained, that is, quartz sand:cement:iron powder:barite powder:water = 3.90:1.00:1.40:1.67:1.37. The basic physical and mechanical parameters of prototype granite and similar materials are shown in Table 2. Through comparison, it is found that although there are errors in the physical and mechanical properties of the model material and the prototype rock, the order of magnitude is basically the same, which meets the requirements of the stress similarity ratio.

**Model test scheme and measuring point arrangement**

According to the ground stress distribution law tested by hydraulic fracturing method and in-situ stress condition selected for theoretical analysis in “Theoretical analysis model” section, the model test scheme of ultra-deep shaft development blasting was determined. The uniform in-situ stress state includes five working conditions with the corresponding excavation depth H = 0m, 500m, 1000m, 1500m and 2000m, the initial loading stress

State of stress	Model conditions	Buried depthH/m	Ground stress in test/MPa
No ground stress	M0	0	$\sigma_H = \sigma_h = \sigma_v = 0$
Uniform ground stresses ( $k = 1$ )	M1	500	$\sigma_H = \sigma_h = 0.21; \sigma_v = 0.13$
	M2	1000	$\sigma_H = \sigma_h = 0.34; \sigma_v = 0.27$
	M3	1500	$\sigma_H = \sigma_h = 0.46; \sigma_v = 0.40$
	M4	2000	$\sigma_H = \sigma_h = 0.58; \sigma_v = 0.54$

**Table 3.** Model test scheme of ultra-deep shaft development blasting.

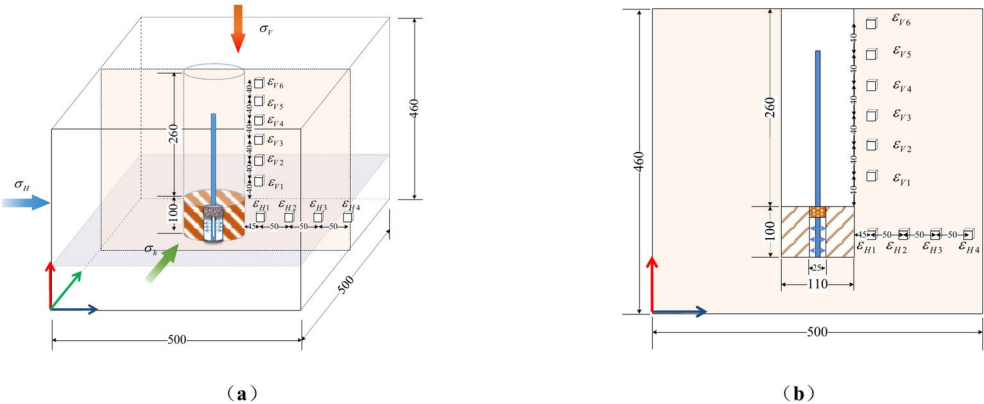


**Fig. 7.** Strain brick layout scheme of ultra-deep shaft development blasting model test (unit: mm): (a) Three-dimensional view; (b) Vertical profile.

in the horizontal direction was calculated according to the average value of the maximum horizontal principal stress and the minimum horizontal principal stress, as shown in Table 3.

The in-situ stress loading value can be loaded according to the design. By adjusting the pressure gauge on the hydraulic pump station to achieve the required loading stress under different working conditions. Compared with the stress distribution law of the original rock<sup>32</sup>, it can be found that the various working conditions of the model test design are similar to the in-situ stress distribution law of the field test.

To test the propagation and attenuation law of stress wave in surrounding rock of ultra-deep shaft during the blasting disturbance model test, considering that the shaft model is a symmetrical structure, only strain bricks were arranged on one side of the shaft. Four strain bricks H1, H2, H3 and H4 were arranged horizontally in the surrounding rock of the shaft, and the placement position was 150 mm from the bottom surface of the model sample. Six strain bricks V1, V2, V3, V4, V5 and V6 were arranged in the vertical direction of the surrounding rock of the shaft, and they were arranged at equal intervals in the vertical direction parallel to the shaft axis. The location of the specific strain brick is shown in Fig. 7. The strain brick is a self-made sensor with the function of synchronous acquisition of radial and hoop strain. Its size is 20 mm × 20 mm × 20 mm. The material properties of the strain brick are the same as those of the surrounding rock. BX120-3AA strain gauges were bonded along the radial and hoop directions of the strain brick top surface, and sealed with sealant. During the test, two DH5922 D portable dynamic signal test and analysis systems were used to synchronously collect strain waves in the surrounding rock of the shaft.

Steps of model test

1. According to the mix ratio of model materials, the materials were weighed in turn and stirred evenly with a mixer.
2. Model test molds were assembled, then similar materials were layered filled, and layered pouring thickness was controlled in 5–10 cm. Horizontal strain bricks were embedded in the filling to 125 mm height. Then, PVC pipes for prefabricated shafts and blastholes were installed in the center of the model.
3. With the increase of the filling height, the strain bricks arranged in the vertical direction were embedded in turn, and the strain brick leads were all drawn from the top of the model.
4. After the model was filled, it was hoisted to the true triaxial loading system using a small gantry after curing. The surface around the sample was coated with a layer of coupling agent with a thickness of 4–6 mm to eliminate the influence of boundary effect and achieve non-reflective boundary conditions.
5. Debugging the hydraulic oil pump and high-pressure gas blasting impact system, using a multimeter to detect whether the strain brick is damaged, and connecting the dynamic signal test and analysis system in turn. In order to ensure the validity of test data and eliminate signal interference, the sampling frequency is 200 kHz. The strain gauge is grounded, and balance zeroing is carried out before the load is applied.

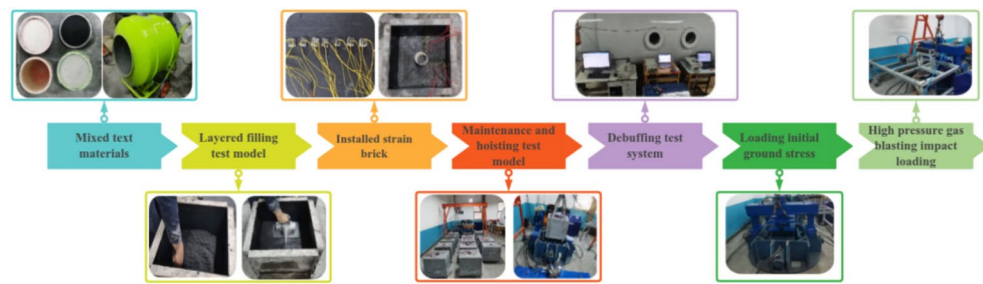


**Fig. 8.** Flow chart of model test.

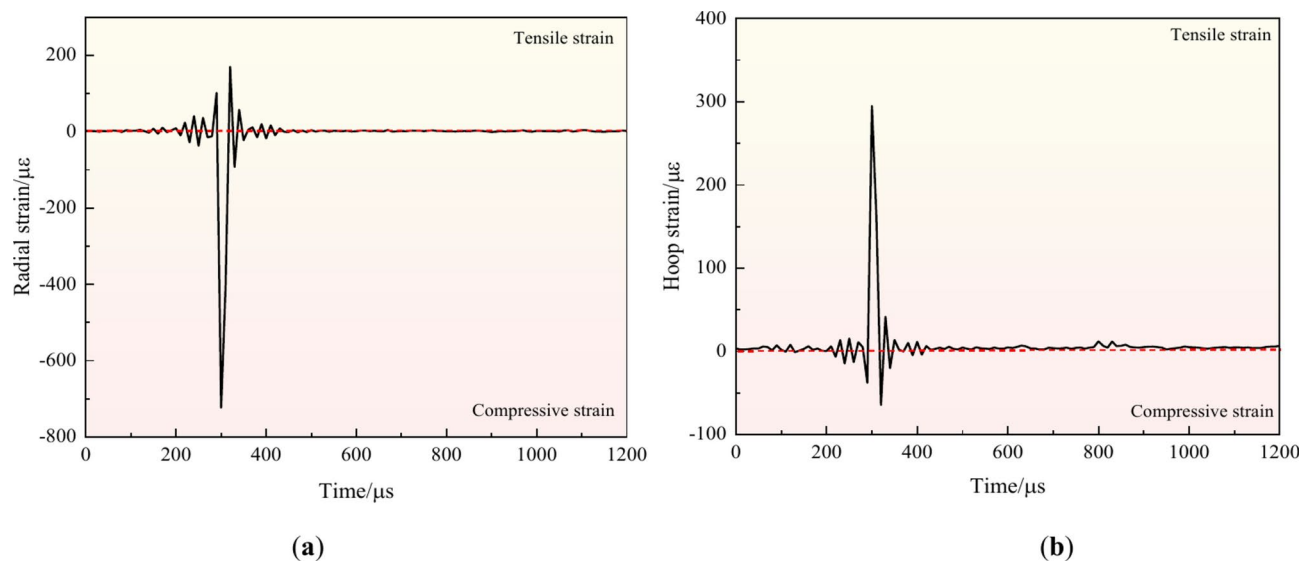


**Fig. 9.** Typical blasting strain wave signals in surrounding rock of shaft model: (a) Radial strain wave signal; (b) Hoop strain wave signal.

6. According to the initial loading stress designed in Table 3, the test model was pressurized and stabilized in turn to ensure that the model meets the requirements of the initial ground stress.
7. The impact pressure of the numerical control pressure gauge was set. When the pressure in the pressure kettle reaches the set value, the electromagnetic valve starts to realize the blasting impact loading, and the strain measuring points were collected and processed. The specific test process is shown in Fig. 8.

## Analysis and discussion of model test results

### Blasting strain wave signal

The propagation law of blasting stress wave in the surrounding rock of shaft under the influence of different ground stresses was mainly explored in this experiment, so it is very important to choose a reasonable blasting impact pressure. Combined with the experimental experience accumulated by the research group and several tests<sup>38,39,44</sup>, it is found that the blasting area in the center of the shaft can be effectively crushed when the impact pressure is designed to be 10–30 MPa, meanwhile it can ensure the effectiveness of the blasting strain wave signal, so the blasting impact pressure selected for each working condition in the model experiment was 10 MPa. According to the strain brick layout scheme in Fig. 7, the dynamic strain measuring points were mainly arranged in the middle area of blasting (> 7 times the radius of blasting hole). When blasting loading was carried out, the typical blasting strain waves collected in the radial and hoop directions of the surrounding rock of the shaft are shown in Fig. 9. The peak data of blasting strain wave collected by dynamic strain measuring points in the horizontal and vertical directions of the shaft model are shown in Table 4 (non-effective data is expressed as '-').

From Fig. 9, it can be seen that the waveform signals include tensile strain and compressive strain, and the compressive strain is mainly in the radial direction, and the tensile strain is mainly in the hoop direction. The duration of the explosion stress wave caused by the blasting impact of high-pressure gas is 200–400 μs, which mainly includes the fluctuation stage in the initial stage of high-pressure gas pressurization, the sudden increase stage of strain stress induced by the superposition of high-pressure gas and stress wave, and the attenuation stage of stress wave. Compared with the blasting stress wave evolution law drawn by the empirical formula of explosive detonation load in the existing literature<sup>9</sup>, the dynamic response generated in the blasting test is obvious, and the



Working condition	Strain gauge direction	Explosion peak strain of each measuring point/ $\mu\epsilon$									
		$\epsilon_{H1}$	$\epsilon_{H2}$	$\epsilon_{H3}$	$\epsilon_{H4}$	$\epsilon_{V1}$	$\epsilon_{V2}$	$\epsilon_{V3}$	$\epsilon_{V4}$	$\epsilon_{V5}$	$\epsilon_{V6}$
M0	Radial direction	-177.37	-111.97	-87.77	-60.02	-160.33	-102.15	-78.26	-	-43.22	-30.87
	Hoop direction	426.07	294.90	136.61	118.15	225.34	180.24	132.94	110.11	80.34	-
M1	Radial direction	-407.96	-203.10	-159.15	-104.34	-200.03	-157.86	-	-85.89	-59.01	-35.36
	Hoop direction	410.98	257.92	135.16	102.18	187.19	150.70	120.00	109.89	70.64	55.34
M2	Radial direction	-444.63	-298.13	-213.46	-107.02	-234.38	-175.25	-142.48	-94.97	-63.74	-
	Hoop direction	322.32	255.43	117.91	93.11	166.14	134.13	100.57	74.56	69.59	50.56
M3	Radial direction	-589.34	-322.13	-231.21	-154.57	-385.16	-261.15	-192.24	-160.98	-	-90.44
	Hoop direction	311.39	253.61	111.28	85.69	157.31	118.15	80.89	-	52.26	47.87
M4	Radial direction	-723.35	-445.09	-274.93	-	-560.75	-420.33	-356.82	-212.63	-	-98.26
	Hoop direction	289.11	195.38	96.99	-	128.35	97.21	64.53	50.74	47.57	37.43

Table 4. Explosion peak strain at each measuring point of shaft model.

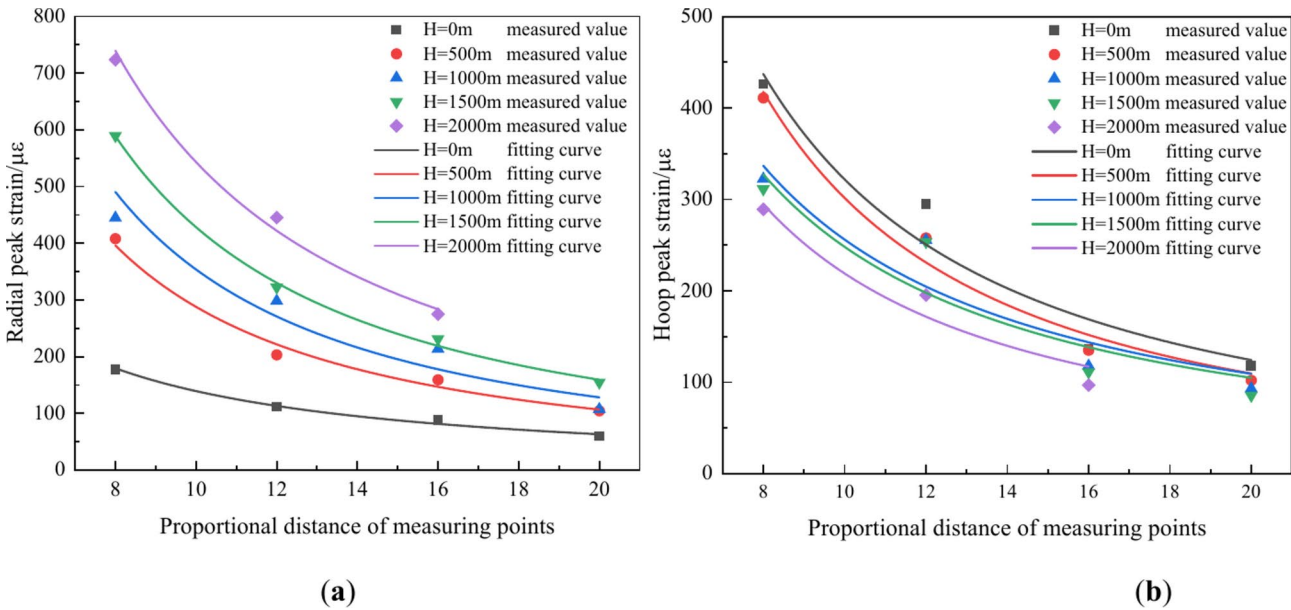


Fig. 10. Relationship curve between explosion peak strain and proportional distance of each measuring point in horizontal direction: (a) Radial peak strain; (b) Hoop peak strain.

validity and reliability of the blasting test results are higher. Generally, the simulated blast source can reflect the time-course variation of blasting pressure. However, due to its low detonation velocity and low energy release, the loading rate is relatively small. Nevertheless, it still belongs to the category of impact loads. The high-pressure gas blast source can be regarded as a low-detonation-velocity and low-equivalent-explosive for regular research and qualitative discussion.

It can be seen from Table 4 that the explosive strain wave in the horizontal and vertical directions of the shaft surrounding rock attenuate with the increase of the propagation distance. The radial peak strain and hoop peak strain of each measuring point in the horizontal direction were slightly larger than the peak strain of each measuring point in the vertical direction. The attenuation rate of radial explosion strain wave was significantly higher than that of hoop explosion strain wave. With the increase of the shaft buried depth or the increase of the ground stress, the radial explosion peak strain increases continuously, while the hoop peak strain decreases continuously. It shows a trend that the radial peak strain is less than the hoop peak strain when in-situ stress is low, while the radial peak strain is greater than the hoop peak strain when in-situ stress is high.

Propagation and attenuation law of horizontal stress wave in surrounding rock

Through the statistical analysis of the explosion strain wave test results at each measuring point in the horizontal direction of the shaft model with different buried depths, the relationship curves between the radial peak strain and the hoop peak strain of each measuring point in the horizontal direction and the proportional distance of the measuring point under different working conditions were obtained, as shown in Fig. 10. Combined with the theoretical analysis results of “Static stress field of surrounding rock under ground stress” and “Dynamic stress field of surrounding rock under blasting load” sections, the evolution law of dynamic stress wave in surrounding

rock at different distances in the horizontal direction of shaft model was obtained by nonlinear regression analysis. The proportional distance is expressed as  $\bar{r} = r/r_0$ ,  $r$  is the distance from the measuring point to the center of the borehole,  $r_0$  is the radius of the borehole designed in the model test, as shown in Table 5.

From Fig. 10, it can be seen that the radial peak strain and hoop peak strain of measuring points in the horizontal direction along the center of shaft model blasted area decrease with the increase of the propagation distance, and because the surrounding rock close to the blasted area is subjected to strong blasting disturbance, the strain wave attenuation of the measuring points in the near area is faster, and the strain wave attenuation rate gradually slows down with the increase of the distance. The reason is that in the process of ultra-deep shaft development blasting, the plastic zone or excavation damage zone formed in the surrounding rock of the shaft is large under the coupling effect of deep high stress and blasting dynamic load. The explosion stress wave attenuates rapidly in the range of  $1 \sim 2R_0$ , and then attenuates slowly.

In addition, it can be seen from Fig. 10a that with the continuous increase of the excavation depth of the shaft, the static strain generated by in-situ stress in the radial direction of the shaft surrounding rock increases continuously, and the dynamic radial strain generated by the blasting stress wave is superimposed. The radial peak strain in the surrounding rock of the shaft increases with the increase of in-situ stress, and the radial peak strain of the near-area measuring point increases obviously. It can be seen from Fig. 10b that with the increase of the shaft excavation depth, the static strain generated by in-situ stress in the hoop direction of the shaft surrounding rock is also increasing, but the static hoop strain is opposite to the dynamic hoop strain generated by the blasting stress wave. The direction will cause the hoop peak strain in the surrounding rock of the shaft to decrease with the increase of in-situ stress, but the reduction of different measuring points is not much different. Compared with the theoretical analysis results of the stress superposition effect around the blasting hole in Fig. 5, it can be seen that the coupling effect of in-situ stress and the blasting dynamic load is strong in the near area of the shaft surrounding rock. With the continuous attenuation of the blasting stress wave, the effect of in-situ stress on far area is greatly. Therefore, it will cause the phenomenon that the radial peak strain of the measuring point in the near area around the shaft increases with the increase of the in-situ stress, while with the increase of the in-situ stress, the radial peak strain of the measuring point in the far area increases and the hoop peak strain decreases.

To quantitatively analyze the attenuation law of dynamic stress wave in the shaft model surrounding rock at different distances in the horizontal direction, according to Formulas (7) and (8), the attenuation law of strain wave was fitted in the form of power exponential function. According to Table 5, corresponding to different buried depths ( $H=0$  m, 500 m, 1000 m, 1500 m, 2000 m), the attenuation indexes of radial peak strain are  $-1.34$ ,  $-1.43$ ,  $-1.46$ ,  $-1.43$ ,  $-1.38$ , respectively, with an average value of  $-1.41$ , and the attenuation indexes of hoop peak strain are  $-1.37$ ,  $-1.45$ ,  $-1.23$ ,  $-1.24$ ,  $-1.33$ , respectively, with an average value of  $-1.32$ . It can be seen that the attenuation rate of radial explosion strain wave is higher than that of hoop strain wave, which conforms to the attenuation index of explosion stress wave  $\alpha = 2 - \mu_d / (1 - \mu_d)$ . In addition, with the increase of in-situ stress, although the radial peak strain of each measuring point increases and the hoop peak strain decreases, the effect of in-situ stress on the attenuation index is not obvious.

Propagation and attenuation law of vertical stress wave in surrounding rock

Through the statistical analysis of the explosion strain wave test results of each measuring point in the vertical direction of the shaft model with different buried depths, the relationship curves between the radial peak strain and the hoop peak strain of each measuring point in the vertical direction and the distance of the measuring point under different working conditions were obtained, as shown in Fig. 11. In addition, the evolution law of dynamic stress wave in the shaft model surrounding rock in the vertical direction was fitted in the form of power exponential function, as shown in Table 6.

It can be seen from Fig. 10 that the relationship between the explosion peak strain and the proportional distance of each measuring point in the vertical direction of the shaft model is similar to that in the horizontal direction, and the explosion peak strain also decays with the increase of the proportional distance for each measuring point. The radial peak strain in the surrounding rock increases with the increase of in-situ stress, and the hoop peak strain decreases with the increase of in-situ stress.

According to the fitting results of the dynamic stress wave attenuation law in the shaft model surrounding rock at different distances in the vertical direction in Table 6, corresponding to different buried depths ( $H=0$  m, 500 m, 1000 m, 1500 m, 2000 m), the attenuation indexes of the radial peak strain are  $-1.90$ ,  $-1.99$ ,  $-1.81$ ,  $-1.68$ ,  $-2.08$ , and the average value is  $-1.89$ . The attenuation indexes of the hoop peak strain are  $-1.44$ ,  $-1.42$ ,

Working condition	Buried depth H/m	Attenuation law of radial peak strain	Attenuation law of hoop peak strain
M0	0	$\sigma_r = 4912.38\bar{r}^{-1.34} \left(R^2 = 0.9889\right)$	$\sigma_\theta = 7576.24\bar{r}^{-1.37} \left(R^2 = 0.9248\right)$
M1	500	$\sigma_r = 7784.07\bar{r}^{-1.43} \left(R^2 = 0.9817\right)$	$\sigma_\theta = 8694.93\bar{r}^{-1.45} \left(R^2 = 0.9720\right)$
M2	1000	$\sigma_r = 10296.13\bar{r}^{-1.46} \left(R^2 = 0.8878\right)$	$\sigma_\theta = 4326.73\bar{r}^{-1.23} \left(R^2 = 0.8459\right)$
M3	1500	$\sigma_r = 11454.53\bar{r}^{-1.43} \left(R^2 = 0.9967\right)$	$\sigma_\theta = 4323.21\bar{r}^{-1.24} \left(R^2 = 0.8130\right)$
M4	2000	$\sigma_r = 13107.96\bar{r}^{-1.38} \left(R^2 = 0.9832\right)$	$\sigma_\theta = 4694.56\bar{r}^{-1.33} \left(R^2 = 0.8923\right)$

Table 5. Attenuation law of dynamic stress wave in shaft model surrounding rock in horizontal direction.

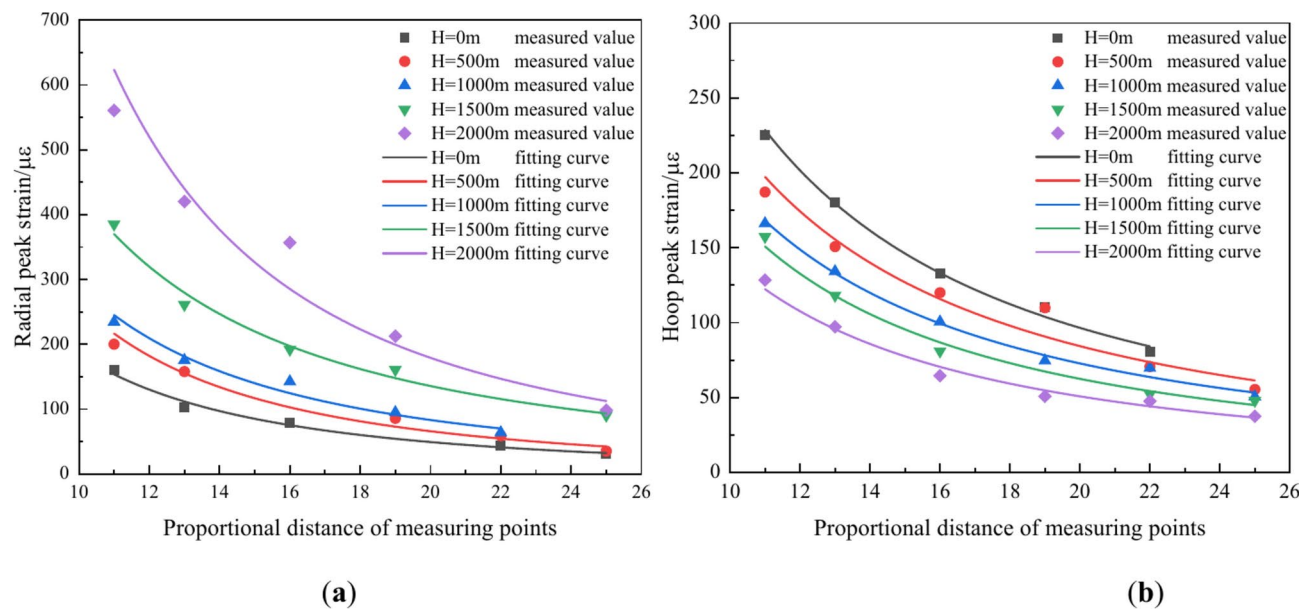


**Fig. 11.** Relationship curve between the explosion peak strain and the proportional distance of each measuring point in the vertical direction: (a) Radial peak strain; (b) Hoop peak strain.

Working condition	Buried depth H/m	Attenuation law of radial peak strain	Attenuation law of hoop peak strain
M0	0	$\sigma_r = 14729.67\bar{r}^{-1.90}$ ( $R^2 = 0.9857$ )	$\sigma_\theta = 7262.49\bar{r}^{-1.44}$ ( $R^2 = 0.9952$ )
M1	500	$\sigma_r = 25604.15\bar{r}^{-1.99}$ ( $R^2 = 0.9730$ )	$\sigma_\theta = 5970.82\bar{r}^{-1.42}$ ( $R^2 = 0.9538$ )
M2	1000	$\sigma_r = 18592.58\bar{r}^{-1.81}$ ( $R^2 = 0.9709$ )	$\sigma_\theta = 4830.54\bar{r}^{-1.40}$ ( $R^2 = 0.9936$ )
M3	1500	$\sigma_r = 20718.65\bar{r}^{-1.68}$ ( $R^2 = 0.9845$ )	$\sigma_\theta = 5179.58\bar{r}^{-1.47}$ ( $R^2 = 0.9896$ )
M4	2000	$\sigma_r = 92745.64\bar{r}^{-2.08}$ ( $R^2 = 0.9242$ )	$\sigma_\theta = 4158.94\bar{r}^{-1.47}$ ( $R^2 = 0.9831$ )

**Table 6.** Attenuation law of dynamic stress wave in shaft model surrounding rock in vertical direction.

– 1.40, – 1.47, – 1.47, and the average value is – 1.43. It also shows that the attenuation rate of radial explosion strain wave is higher than that of hoop strain wave, which is similar to the propagation and attenuation law of dynamic stress wave in horizontal direction. Comparing the stress wave propagation law obtained in the test with the measured results of the surrounding rock dynamic response for the blasting excavation of a highway tunnel ventilation shaft<sup>29</sup>, it is reasonable that the peak strain law of each measuring point with the increase of proportional distance in the surrounding rock vertical direction was fit as exponential decline. However, due to the limitation of the test model, it is not reflected in the length-diameter ratio of the shaft model, and the ventilation shaft in the literature is not an ultra-deep shaft. Therefore, the propagation and attenuation law of the explosion stress wave along the vertical direction in the surrounding rock of the ultra-deep shaft under the action of high ground stress remains to be further studied.

## Conclusions

1. The surrounding rock stress field of ultra-deep shaft development blasting is superimposed composed of the static stress field under the action of deep high stress and the dynamic stress field under the action of blasting load. The static stress field can be analytically calculated according to the theory of elastic mechanics, and the dynamic stress field of surrounding rock needs to be combined with the actual working conditions of ultra-deep shaft millisecond blasting, it can be calculated according to the attenuation law of blasting stress wave, after the blasting load on the blasting excavation boundary of each section is equivalent. According to the superposition effect, it can be seen that the dynamic stress generated by the blasting load in the radial direction is the same as the static stress generated by the ground stress, which increases with the increase of in-situ stress. In the hoop direction, the dynamic stress is opposite to the static stress. In-situ stress weakens the tensile stress generated by the blasting load in the hoop direction, thereby inhibiting the expansion of blasting cracks and effectively reducing the blasting damage range at the excavation boundary of the shaft.
2. A physical model test system with the combined loading function of three-dimensional static stress and explosion shock was developed. Based on the true triaxial static loading system, the boundary conditions of the

three-dimensional in-situ stress in the shaft model are realized. Based on the high-pressure gas blasting impact system, the application of blasting impact load is realized. The monitoring of blasting strain wave shows that the blasting strain wave contains tensile phase and compressive phase, and the radial direction strain is dominated by compressive strain, and the hoop direction strain is dominated by tensile strain. The dynamic response generated in the blasting test is obvious, and the validity and reliability of the blasting test results are higher. It shows that the high-pressure gas blast source can be regarded as a low-detonation-velocity and low-equivalent-explosive for regular research and qualitative discussion.

3. In the process of ultra-deep shaft development blasting, the surrounding rock blasting stress waves in the horizontal and vertical directions decay in the form of power exponential function with the increase of propagation distance, and the attenuation index in the vertical direction is greater than that in the horizontal direction. In addition, with the increase of in-situ stress, the radial peak strain in the surrounding rock increases continuously, while the hoop peak strain in the surrounding rock decreases continuously. Because the radial peak strain increases greatly in the range of  $1 \sim 2R_0$ , the plastic zone or excavation damage zone formed in the surrounding rock is large, and the explosion stress wave attenuates rapidly in the range of  $1 \sim 2R_0$ , and then attenuates slowly. Because the reduction of the hoop peak strain at different measuring points is not much different, the effect of in-situ stress on the attenuation index is not obvious.

## Data availability

All data generated or analysed during this study are included in this published article.

Received: 21 November 2024; Accepted: 30 January 2025

Published online: 13 February 2025

## References

1. Cai, M. & Brown, E. Challenges in the mining and utilization of deep mineral resources. *Engineering* **3**(4), 432–433. <https://doi.org/10.1016/j.ENG.2017.04.027> (2017).
2. Zhao, X. Basic theory and development trends of ultra-deep shaft construction. *Metal Mine* **04**, 1–10. <https://doi.org/10.19614/j.cnki.jsks.201804001> (2018) (in Chinese).
3. Li, P. et al. In situ stress state of the northwest region of the Jiaodong Peninsula, China from overcoring stress measurements in three gold mines. *Rock Mech. Rock Eng.* **52**(11), 4497–4507. <https://doi.org/10.1007/s00603-019-01827-3> (2019).
4. Yang, R. et al. Statistics and analysis on blasting excavation parameters of vertical shaft in China's recent 50 years. *J. China Univ. Min. Technol.* **51**(06), 1031–1044. <https://doi.org/10.1007/s00603-024-04106-y> (2022) (in Chinese).
5. Hall, A. et al. Preconditioning blasting for rockburst control in a deep shaft sink. *Int. J. Rock Mech. Min. Sci.* **181**, 105841. <https://doi.org/10.1016/j.ijrmms.2024.105841> (2024).
6. Walton, G. et al. Investigation of shaft stability and anisotropic deformation in a deep shaft in Idaho, United States. *Int. J. Rock Mech. Min. Sci.* **105**, 160–171. <https://doi.org/10.1016/j.ijrmms.2018.03.017> (2018).
7. Zhao, X. & Li, Y. Estimation of support requirement for a deep shaft at the Xincheng Gold Mine, China. *Bull. Eng. Geol. Environ.* **80**(9), 6863–6876. <https://doi.org/10.1007/s10064-021-02350-y> (2021).
8. Zhang, C., Hu, F. & Zou, S. Effects of blast induced vibrations on the fresh concrete lining of a shaft. *Tunnell. Undergr. Space Technol.* **20**(4), 356–361. <https://doi.org/10.1016/j.tust.2005.01.001> (2005).
9. Yi, C., Johansson, D. & Greberg, J. Effects of in-situ stresses on the fracturing of rock by blasting. *Comput. Geotech.* **104**, 321–330. <https://doi.org/10.1016/j.compgeo.2017.12.004> (2018).
10. Tao, J. et al. Effects of in-situ stresses on dynamic rock responses under blast loading. *Mech. Mater.* **145**, 103374. <https://doi.org/10.1016/j.mechmat.2020.103374> (2020).
11. Li, X. et al. Numerical study on the behavior of blasting in deep rock masses. *Tunnell. Undergr. Space Technol.* **113**, 103968. <https://doi.org/10.1016/j.tust.2021.103968> (2021).
12. He, C., Yang, J. & Yu, Q. Laboratory study on the dynamic response of rock under blast loading with active confining pressure. *Int. J. Rock Mech. Min. Sci.* **102**, 101–108. <https://doi.org/10.1016/j.ijrmms.2018.01.011> (2018).
13. Peng, L. et al. Experimental study on the influence of biaxial confining pressure on dynamic cracks and its inter-action with blasting stress wave. *Theoret. Appl. Fract. Mech.* **123**, 103719. <https://doi.org/10.1016/j.tafmec.2022.103719> (2023).
14. Yang, L. et al. Numerical and experimental study of the presplit blasting failure characteristics under compressive stress. *Soil Dyn. Earthq. Eng.* **149**, 106873. <https://doi.org/10.1016/j.soildyn.2021.106873> (2021).
15. Jayasinghe, L. et al. Numerical investigation into the blasting-induced damage characteristics of rocks considering the role of in-situ stresses and discontinuity persistence. *Comput. Geotech.* **116**, 103207. <https://doi.org/10.1016/j.compgeo.2019.103207> (2019).
16. Wen, W. et al. Numerical study on the rock-breaking mechanism and stress superposition effect of double-hole delayed blasting in deep reservoirs. *Int. J. Geomech.* <https://doi.org/10.1061/IJGNALGMENG-8858> (2024).
17. Xie, L. et al. Damage evolution mechanisms of rock in deep tunnels induced by cut blasting. *Tunnell. Undergr. Space Technol.* **58**, 257–270. <https://doi.org/10.1016/j.tust.2016.06.004> (2016).
18. Qiu, J. et al. Numerical investigation on the stress evolution and failure behavior for deep roadway under blasting disturbance. *Soil Dyn. Earthq. Eng.* **137**, 106278. <https://doi.org/10.1016/j.soildyn.2020.106278> (2020).
19. Wang, Y. et al. Dynamic response of cylindrical deep buried tunnels in unsaturated soil under axisymmetric explosion loading. *Soil Dyn. Earthq. Eng.* **175**, 108261. <https://doi.org/10.1016/j.soildyn.2023.108261> (2023).
20. Hong, Z. et al. Investigation on overbreak and underbreak of pre-stressed tunnels under the impact of decoupled charge blasting. *Int. J. Impact Eng.* **182**, 104784. <https://doi.org/10.1016/j.ijimpeng.2023.104784> (2023).
21. Li, X. et al. Numerical study on the effect of in-situ stress on smoothwall blasting in deep tunnelling. *Undergr. Space* **11**, 96–115. <https://doi.org/10.1016/j.undsp.2022.11.003> (2023).
22. Han, H. et al. Combined finite-discrete element modelling of rock fracture and fragmentation induced by contour blasting during tunnelling with high horizontal in-situ stress. *Int. J. Rock Mech. Min. Sci.* **127**, 104214. <https://doi.org/10.1016/j.ijrmms.2020.104214> (2020).
23. Yang, J. et al. 2D numerical analysis of rock damage induced by dynamic in-situ stress redistribution and blast loading in underground blasting excavation. *Tunnell. Undergr. Space Technol.* **70**, 221–232. <https://doi.org/10.1016/j.tust.2017.08.007> (2017).
24. Zhang, T. et al. Characteristics of the elevation amplification effect of vibration velocity in rock surrounding underground cavities under different stress conditions. *Soil Dyn. Earthq. Eng.* **165**, 107704. <https://doi.org/10.1016/j.soildyn.2022.107704> (2023).
25. Zhao, X. et al. Analysis and application of disturbance stress reaction mechanism of surrounding rock during sinking ultra-deep shaft. *Disast. Prev. Tunnel Undergr. Eng.* **2**(04), 19–28. <https://doi.org/10.1007/s00603-024-04106-y> (2020) (in Chinese).
26. Shan, R. et al. Damage model of frozen vertical shaft concrete under blasting load in Northwest China. *J. China Coal Soc.* **40**(03), 522–527. <https://doi.org/10.13225/j.cnki.jccs.2014.1816> (2015) (in Chinese).



27. Shan, R. et al. Experimental study on blasting vibration and damage characteristics on frozen shaft wall. *Chin. J. Rock Mech. Eng.* **34**(S2), 3732–3741. <https://doi.org/10.13722/j.cnki.jrme.2015.0603> (2015) (in Chinese).
28. Hu, L. et al. Characteristics of the microseismicity resulting from the construction of a deeply-buried shaft. *Tunnell. Undergr. Space Technol.* **85**, 114–127. <https://doi.org/10.1016/j.tust.2018.12.016> (2019).
29. Xie, H. et al. Dynamic response of rock mass subjected to blasting disturbance during tunnel shaft excavation: A field study. *Geomech. Geophys. Geo-Energy Geo-Resour.* <https://doi.org/10.1007/s40948-022-00358-6> (2022).
30. Li, X., Meng, J. & Xu, P. Study of blasting seismic effects of cable shaft in Xiluodu hydropower station. *Rock Soil Mech.* **32**(02), 474–480. <https://doi.org/10.3969/j.issn.1000-7598.2011.02.026> (2011) (in Chinese).
31. Zuo, J. *Experimental Study on Sectional Cutting and Directional Damage Control of Vertical Shaft Deep Hole* (China University of Mining & Technology, 2020) (in Chinese).
32. Hou, K. et al. Application of different in-situ stress test methods in the area of 2005 m shaft construction of Sanshandao gold mine and distribution law of in-situ stress. *Rock Soil Mech.* **43**(04), 1093–1102. <https://doi.org/10.3969/j.issn.1000-7598.2011.02.026> (2022) (in Chinese).
33. Xiao, P. et al. Characteristics and mechanism of rockburst at five deep gold mines in Jiaodong Peninsula of China. *Int. J. Rock Mech. Min. Sci.* **171**, 105574. <https://doi.org/10.1016/j.ijrmms.2023.105574> (2023).
34. Ding, J. et al. Numerical study on rock blasting assisted by in-situ stress redistribution. *Tunnell. Under-ground Space Technol.* **153**, 106022. <https://doi.org/10.1016/j.tust.2024.106022> (2024).
35. Dai, J. *Rock Dynamic Characteristics and Blasting Theory* (Metallurgical Industry Press, 2013) (in Chinese).
36. Lu, W. et al. An equivalent method for blasting vibration simulation. *Simul. Model. Pract. Theory* **19**(9), 2050–2062. <https://doi.org/10.1016/j.simpat.2011.05.012> (2011).
37. Chen, Z. et al. A novel carbon dioxide phase transition rock breaking technology: Theory and application of non-explosive blasting. *Processes* **10**(11), 2434. <https://doi.org/10.3390/pr10112434> (2022).
38. Yan, S. et al. Experimental study on dynamic response and damage evolution of coal under shocks by multiple high-pressure air blasting. *Geofluids* **2022**, 1–12. <https://doi.org/10.1155/2022/2033679> (2022).
39. Yang, X. et al. Study on the stress field and crack propagation of coal mass induced by high-pressure air blasting. *Minerals* **12**(3), 300. <https://doi.org/10.3390/min12030300> (2022).
40. Feng, X. et al. A novel large-scale three-dimensional physical model experimental system for deep underground engineering. *Rock Mech. Rock Eng.* **56**(11), 8395–8413. <https://doi.org/10.1007/s00603-023-03495-w> (2023).
41. Zhu, G. et al. Physical model study on brittle failure of pressurized deep tunnel with support system. *Rock Mech. Rock Eng.* **56**(12), 9013–9033. <https://doi.org/10.1007/s00603-023-03541-7> (2023).
42. Einstein, H. Physical modelling in rock mechanics and rock engineering. *Rock Mech. Rock Eng.* <https://doi.org/10.1007/s00603-024-04106-y> (2024).
43. Zhou, H. et al. Experimental study of rockburst model material with low-strength and high-brittleness. *Rock Soil Mech.* **40**(06), 2039–2049. <https://doi.org/10.16285/j.rsm.2017.1861> (2019) (in Chinese).
44. Chu, H. et al. A simulation experimental study on high pressure air blasting of coal. *J. Vib. Shock* **41**(20), 54–60. <https://doi.org/10.13465/j.cnki.jvs.2022.20.007> (2022) (in Chinese).

## Acknowledgements

This research was funded by the National Key Research and Development Program of China (Grant No. 2023YFC2907202), the State Key Program of National Natural Science of China (Grant No. 52130403) and the open fund of Key Laboratory of Intelligent Construction and Safety Operation and Maintenance of Underground Engineering in Henan Province (Grant No. KFKT2024-01)

## Author contributions

Bo Sun: Conceptualization, Data curation, Writing-original draft. Xiaolin Yang: Investigation, Methodology, Writing-review & editing, Funding acquisition. Huaibao Chu: Writing-review & editing, Fengbin Chen: Writing-review & editing, Jinxing Wang: Writing-review & editing, Peng Guo and Zhikai Cheng: Writing-review & editing.

## Declarations

## Competing interests

The authors declare no competing interests.

## Additional information

**Correspondence** and requests for materials should be addressed to B.S.

**Reprints and permissions information** is available at [www.nature.com/reprints](http://www.nature.com/reprints).

**Publisher's note** Springer Nature remains neutral with regard to jurisdictional claims in published maps and institutional affiliations.

**Open Access** This article is licensed under a Creative Commons Attribution-NonCommercial-NoDerivatives 4.0 International License, which permits any non-commercial use, sharing, distribution and reproduction in any medium or format, as long as you give appropriate credit to the original author(s) and the source, provide a link to the Creative Commons licence, and indicate if you modified the licensed material. You do not have permission under this licence to share adapted material derived from this article or parts of it. The images or other third party material in this article are included in the article's Creative Commons licence, unless indicated otherwise in a credit line to the material. If material is not included in the article's Creative Commons licence and your intended use is not permitted by statutory regulation or exceeds the permitted use, you will need to obtain permission directly from the copyright holder. To view a copy of this licence, visit <http://creativecommons.org/licenses/by-nc-nd/4.0/>.

© The Author(s) 2025